Available online at www.sciencedirect.com
ScienceDirect
Polymer 48 (2007) 3771–3780
polymer
www.elsevier.com/locate/polymer

A parametric study into the morphology of polystyrene-*co*-methyl methacrylate foams using supercritical carbon dioxide as a blowing agent

L.J.M. Jacobs*, K.C.H. Danen, M.F. Kemmere, J.T.F. Keurentjes

Process Development Group, Department of Chemical Engineering and Chemistry, Eindhoven University of Technology, P.O. Box 513, 5600 MB Eindhoven, The Netherlands

Received 2 February 2007; received in revised form 1 May 2007; accepted 3 May 2007
Available online 7 May 2007

Abstract

In this study the foaming of poly(styrene-*co*-methyl methacrylate) (SMMA) using supercritical carbon dioxide is investigated. The effect of different foaming parameters such as temperature and pressure is studied in a quantitative and systematic way, with the aim to control and predict the resulting foam morphology. It is shown that once the polymer properties, such as the glass transition temperature and the solubility of CO_2 are known, full control of the desired foam morphology can be obtained by a proper selection of temperature, pressure and depressurization rate.

Keywords: Poly(styrene-*co*-methyl methacrylate); Supercritical carbon dioxide; Foam morphology

1. Introduction

Polymeric foams are most commonly used as thermal insulating, comfort cushioning and packaging materials. These materials can be divided into two main groups: the thermoset and the thermoplast foams. Thermoset foams are mainly polyurethane-based and are often produced by applying a chemical foaming agent that decomposes at a certain temperature, generating gas bubbles within the polymer [1]. Thermoplast foams are usually polyethylene- or polystyrene-based and their production process applies a thermally induced phase separation, where a dissolved volatile organic compound (VOC), e.g. pentane, nucleates and evaporates after an increase in temperature. Unfortunately, the VOCs can only be partly recovered, whereas the main part disappears into the environment.

In recent years the interest in green technology has grown enormously, due to the ever more stringent environmental legislation. Supercritical carbon dioxide ($scCO_2$) has turned out to be a very promising solvent for the replacement of VOCs in industry, especially in the production of foams from glassy polymers, like Styrofoam [2–4]. Supercritical carbon dioxide has proven to be a good alternative, because it is relatively inert, nonflammable, cheap and it is generally regarded as safe (GRAS-status). Furthermore, the critical conditions are relatively mild and therefore easily accessible.

The foaming of polymers using $scCO_2$ can roughly be divided into two steps. The first step consists of saturating the polymeric sample with CO_2. This will lead to plasticization and a decrease in the glass transition temperature (T_g) of the polymer [5,6], which is schematically presented in Fig. 1. Furthermore, the polymer will swell due to plasticization. After saturation, a (rapid) depressurization step will induce phase separation and nucleation because of a shift in the thermodynamic equilibrium. Subsequently, cell growth will occur. Because of this, the amount of CO_2 present in the polymer matrix will decrease and the T_g of the polymer will start to increase again. At a certain point, the polymer returns to the glassy state, which means that the matrix vitrifies and cell growth will stop. The vitrification, together with the pressure and temperature at which the polymer is saturated with CO_2, as well as the depressurization rate determines to a large extent the morphology of the foam that will be obtained.

* Corresponding author. Tel.: +31 40 2472884; fax: +31 40 2446104.
E-mail address: l.j.m.jacobs@tue.nl (L.J.M. Jacobs).

0032-3861/$ - see front matter © 2007 Elsevier Ltd. All rights reserved.
doi:10.1016/j.polymer.2007.05.002

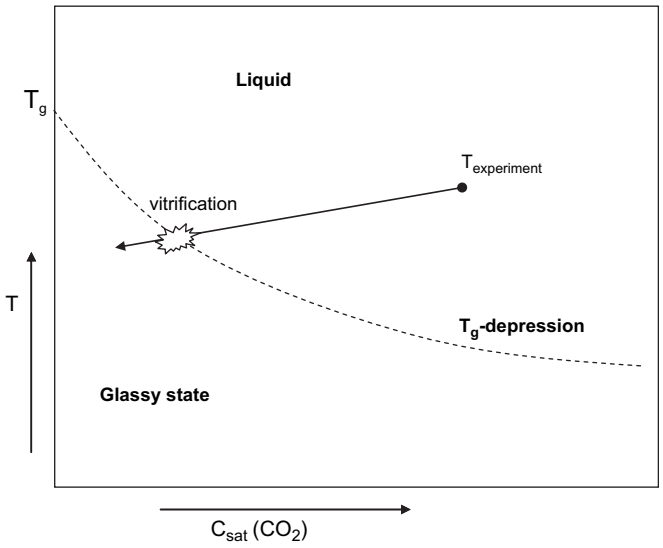

Fig. 1. Schematic representation of the T_g-depression and the vitrification of the polymer matrix during a foaming experiment.

Since the early nineties, a substantial amount of work has been published on the foaming of various polymers and polymer blends using $scCO_2$ [7–12]. Even though most of these publications address the "foaming with CO_2 topic", usually only SEM pictures are presented, together with some general density and cell size information. In order to apply the $scCO_2$-based foaming process on a larger scale, the foaming conditions that yield economically required foam densities need to be investigated. However, this information is hardly available in the literature. Therefore, this study approaches the foaming process at high temperatures and pressures of poly(styrene-*co*-methyl methacrylate) (SMMA) in a quantitative and systematic way, to determine the effect of different foaming parameters, with the aim to control and predict the foam morphology and to produce foams with densities in the same range as commercially available foams. The effect of temperature, pressure and depressurization rate on the foam morphology of SMMA has been analyzed and Voronoi diagrams have been used to determine the average cell area, cell area distribution and the homogeneity of the produced foams. Sorption measurements of carbon dioxide in SMMA have been performed, using a magnetic suspension balance (MSB).

2. Experimental

2.1. Materials

Poly(styrene-*co*-methyl methacrylate) (SMMA) with 40 wt% styrene was purchased from Aldrich Chemical Company. GPC analysis with polystyrene standard indicated a M_n of 76 kg/mol and a polydispersity of 2.2. The glass transition temperature (T_g) as determined by DSC analysis (Perkin–Elmer Pyris Diamond DSC) revealed a T_g of 101 °C. Carbon dioxide (CO_2) (grade 4.5) was obtained from Hoek Loos (Amsterdam, The Netherlands) and was used without further purification.

2.2. Sorption experiments

To determine the CO_2 uptake in the polymer, sorption experiments were performed at the Ruhr University in Bochum, using an MSB (Rubotherm, Germany). The mass uptake of the sample in a high pressure cell was measured with a microbalance, located outside the chamber, using a magnetic coupling to transmit the signal. A more detailed description of the MSB can be found in the literature [13]. The signal of the MSB was corrected for buoyancy effects due to the increase in CO_2 density with increasing pressure. However, the results still had to be corrected for the swelling of the polymer, caused by the sorption of CO_2, which was estimated using the Sanchez–Lacombe equation of State (SL-EOS).

2.3. Sanchez–Lacombe equation of state

Several papers have already discussed the successful description of polymer–CO_2 sorption and swelling isotherms using the SL-EOS [14–16]. Therefore, this EOS was used to determine the actual sorption values. The SL-EOS expressed in reduced parameters is given by [17–19]:

$$\tilde{\rho}^2 + \tilde{P} + \tilde{T}\left[\ln(1-\tilde{\rho}) + \left(1 - \frac{1}{r}\right)\tilde{\rho}\right] = 0 \tag{1}$$

$$\tilde{\nu} = \frac{1}{\tilde{\rho}} \tag{2}$$

where $\tilde{\rho}$, $\tilde{\nu}$, $\tilde{P}$, $\tilde{T}$ are the reduced density, specific volume, pressure and temperature, respectively, and r expresses the number of lattice sites occupied by a molecule. The reduced parameters are defined as:

$$\tilde{\rho} = \rho/\rho^* \tag{3}$$

$$\tilde{T} = T/T^* \tag{4}$$

$$\tilde{P} = P/P^* \tag{5}$$

$$\tilde{\nu} = \nu/\nu^* \tag{6}$$

$$r = MP^*/RT^*\rho^* \tag{7}$$

where M is the molecular weight, R is the ideal gas constant, T, P, ν, and ρ, are the temperature, pressure, molar volume and density, respectively. The parameters with an asterisk (*) indicate the characteristic SL parameters of the components. The SL-EOS can be used for mixtures, by using the following mixing rules:

$$P^* = \sum_i \sum_j \varphi_i \varphi_j P^*_{ij} \tag{8}$$

$$P_{ij}^{*} = \left(1 - k_{ij}\right)\sqrt{P_i^{*}P_j^{*}} \tag{9}$$

$$T^{*} = P^{*}\sum_i \left(\varphi_i^0 T_i^{*}\right)/P_i^{*} \tag{10}$$

$$r_i^0 v_i^{*} = r_i v^{*} \tag{11}$$

$$v^{*} = \sum_i \varphi_i^0 v_i^{*} \tag{12}$$

$$1/r = \sum_i \varphi_i/r_i \tag{13}$$

$$\varphi_i^0 = \left(\varphi_i P_i^{*}/T_i^{*}\right)/\sum_i \left(\varphi_j P_j^{*}/T_j^{*}\right) \tag{14}$$

$$\varphi_i = \left(w_i/\rho_i^{*}\right)/\sum_i \left(w_j/\rho_j^{*}\right) \tag{15}$$

where φ_i and w_i represent the volume and weight fraction of component i in the mixture ij, respectively. The pure state of a component is denoted with the superscript "0". The interaction parameter k_{ij} was used to optimize the model for reaching chemical equilibrium:

$$\mu_i^{\text{gas}} = \mu_i^{\text{polymer}} \tag{16}$$

which states that the chemical potential of the components in the gas phase needs to be equal to the chemical potential of the components in the polymer phase. The chemical potential of CO_2, denoted as "1", in the polymer phase, denoted as "2", is given by:

$$\begin{aligned}\mu_1^{\text{polymer}} = RT\Big[\ln\varphi_1 + (1 - r_1/r_2)\varphi_2 + r_1^0\tilde{\rho}\varphi_2^2\Big(\left(P_1^{*} + P_2^{*} - 2P_{12}^{*}\right)/ \\ \times\left(P_1^{*}\tilde{T}_1\right)\Big)\Big] + r_1^0 RT\Big[\Big(-\tilde{\rho} + \tilde{P}_1\tilde{\nu}\Big)\Big/\tilde{T}_1 \\ + \tilde{\nu}\Big(\Big(1 - \tilde{\rho}\Big)\ln\Big(1 - \tilde{\rho}\Big) + \tilde{\rho}/r_1^0\ln\tilde{\rho}\Big)\Big]\end{aligned} \tag{17}$$

Assuming that no polymer will dissolve in the gas phase, the chemical potential for the gas phase reduces to:

$$\begin{aligned}\mu_1^{\text{gas}} = r_1^0 RT\Big[\Big(-\tilde{\rho}_1 + \tilde{P}_1\tilde{\nu}_1\Big)\Big/\tilde{T}_1 + \tilde{\nu}_1\Big((1 - \tilde{\rho}_1) \\ \times\ln(1 - \tilde{\rho}_1) + \tilde{\rho}_1/r_1^0\ln\tilde{\rho}_1\Big)\Big]\end{aligned} \tag{18}$$

The predicted swelling factor S_w of the polymer can be calculated with the parameters obtained from the SL-EOS, using the following equation [20]:

$$S_w = \frac{\rho_{\text{polymer}}/\rho_{\text{mix}}}{1 - x} \tag{19}$$

where ρ_{polymer}, ρ_{mix} and x represent the density of the pure polymer, the density of the polymer–CO_2 mixture and the mass fraction CO_2, respectively.

For correcting each sorption isotherm, the k_{ij} has to be calculated. The accuracy of the corrected sorption values will improve if a different k_{ij} is calculated for each pressure value [21]. In this study, however, it was sufficient to know the trends of the solubility versus pressure. Therefore, only the measured sorption at 150 bar was used to calculate the k_{ij} of each isotherm. This k_{ij} was used to calculate the predicted sorption and swelling by the SL-EOS. The measured points were corrected according to Eq. (20):

$$m_{\text{corr}} = m_0 + \rho_{\text{fluid}}\Delta V_{\text{polymer}} \tag{20}$$

where m_{corr}, $\Delta V_{\text{polymer}}$, ρ_{fluid} and m_0 represent the corrected values, the difference in polymer volume, the density of CO_2 and the absolute sorption, respectively. A new value for k_{ij} was determined using the corrected uptake, together with the corresponding calculated SL sorption and swelling isotherms. This procedure was repeated until a good agreement was reached between the corrected points and the isotherm predicted by the SL-EOS.

2.4. Foaming experiments

Foaming experiments were performed in a stainless steel high pressure vessel of 67 mL, equipped with a pressure sensor (Keller piezo-resistive pressure transmitter PA-23). A pump (ISCO Seringe 100DX) controlled the pressure of the system. The temperature was regulated using a thermostat bath (Huber Polystat CC1). The experimental setup is schematically shown in Fig. 2.

Rapid expansion experiments were performed with polymeric samples equilibrated at various temperatures and pressures. A set of experiments was carried out at different depressurization rates, after the system was equilibrated at a pre-set temperature and pressure. The pressure decay in time was measured using a Penlab module.

2.5. Morphology characterization

The bulk densities were determined using a pycnometer, a calibrated flask with a fixed volume. The cell structure of the polymeric foam was determined by Scanning Electron Microscopy (SEM) (Jeol, JSM-500), after cryofracturing and

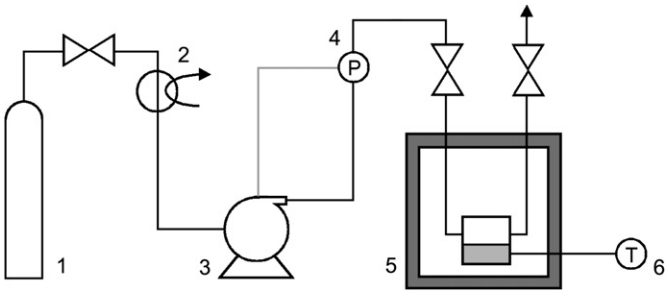

Fig. 2. Schematic representation of the experimental setup with (1) carbon dioxide feed (2) feed cooling (3) pump (4) pressure indicator (5) high pressure thermostated vessel (6) temperature indicator.

sputter coating of the sample with a gold layer of approximately 55 nm. The SEM pictures were converted into a Voronoi diagram, by first converting the picture into an image with only the perimeter of the cells. This image was then used to determine the center of each cell. The x and y coordinates of the centers were used to construct the Voronoi diagram. A more detailed description of this procedure and the analysis using the cell size distributions and homogeneity parameters can be found in the literature [22]. The area (A) of each cell of the Voronoi diagram was used to determine the dimensionless homogeneity number HP_A, by dividing the standard deviation σ_A of the area, by its average value, μ_A.

$$HP_A = \frac{\sigma_A}{\mu_A} \tag{21}$$

with

$$\mu_A = \frac{1}{N}\sum_{i=1}^{N} A_i \tag{22}$$

$$\sigma_A = \sqrt{\frac{\sum_{i=1}^{N}(A_i - \mu_A)^2}{N-1}} \tag{23}$$

The smaller the value for HP_A, the more homogeneous the foam morphology will be. At least 100 cells were assessed to allow a valid statistical analysis.

3. Results and discussion

3.1. Sorption experiments and SL-equation of state correction

Sorption measurements have been performed in order to determine the solubility of CO_2 in SMMA. Since a MSB has been used to determine the sorption, the results have been corrected for the swelling with the predictions of the SL-EOS. The characteristic parameters of the pure components used in the SL-EOS can be found in Table 1 [14,23].

Fig. 3 shows the uncorrected sorption isotherms at 90 °C, 120 °C and 150 °C. The downward trends of the isotherms with increasing pressure clearly show the influence of swelling on the measurements, because for PS and PMMA-based polymers it is to be expected that the sorption isotherms would increase with increasing pressure. For correcting each isotherm, the measured sorption at 150 bar has been used to calculate k_{ij}, and the corresponding sorption and swelling predicted by SL-EOS. The final corrected results with the corresponding SL-isotherms are plotted in Fig. 4.

Table 1
Characteristic parameters of SMMA and CO_2 used for the SL-EOS [14,23]

Component	P^* [MPA]	T^* [K]	ρ^* [kg/m^3]
SMMA	438.1	743.0	1195.0
CO_2	427.7	338.7	1405.5

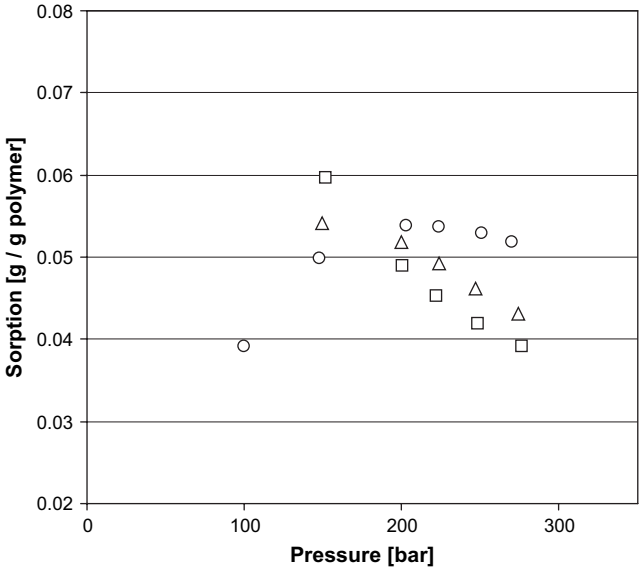

Fig. 3. Measured sorption of CO_2 in SMMA at (□) 90 °C, (△) 120 °C and (○) 150 °C.

It can be seen that as the temperature increases, the amount of CO_2 that can be dissolved in the polymer decreases. Furthermore, the sorption at 120 °C and 150 °C are comparable, indicating a limitation in the amount of CO_2 that can be dissolved in SMMA. No results of CO_2 sorption at high temperatures in SMMA have been reported in the literature. However, it is expected that the sorption for the co-polymer will be a combination of the sorption of the two homopolymers, related to the mass fractions of the different repeating units [24]. Therefore, the sorption results obtained in this study

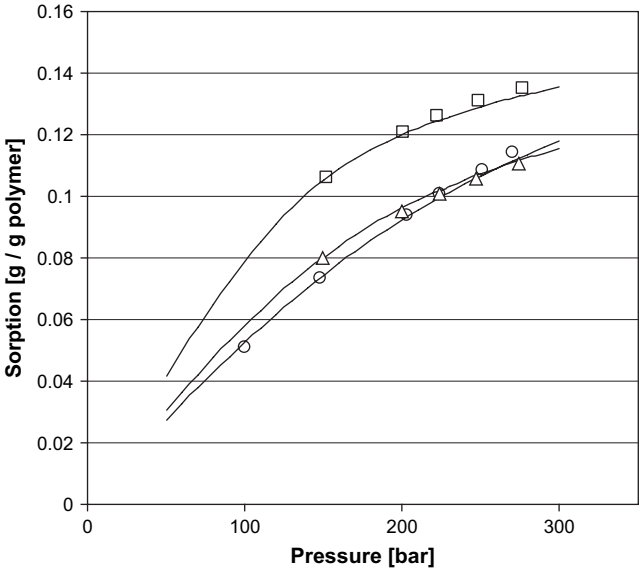

Fig. 4. Corrected CO_2 sorption isotherms of SMMA. k_{ij}((□) 90 °C) = 0.144, k_{ij}((△) 120 °C) = 0.130, k_{ij}((○) 150 °C) = 0.110. The symbols denote the corrected experimental values and the lines denote the isotherms predicted with the SL-EOS.

are what can be expected after comparison to the sorption results for PS and PMMA, reported by Pantoula and Panayiotou [25].

3.2. Foaming experiments

3.2.1. Effect of temperature

The temperature at which the foaming takes place determines the foam morphology to a large extent. Not only does the temperature determine the amount of CO_2 that can be dissolved in the polymer, which in turn is related to the obtained T_g-depression, but it also determines the time available for growth of the cells before the polymer matrix will vitrify due to the transition into the glassy state. This is schematically depicted in Fig. 1.

The effect of temperature is further illustrated by Fig. 5. Here, the results of foaming experiments with a rapid depressurization (<1 s) are displayed, in terms of foam density versus the temperature. At 93 °C the density of the produced foams is much higher than the density of the foams produced at 118 °C, even though the solubility of CO_2 at 90 °C is higher. This indicates a premature stop in cell growth. Fig. 5 also shows that the decrease in density levels off at about 118 °C. Above this temperature a further increase in temperature has little effect on the density, which can be explained by the sorption isotherms. Fig. 4 has already indicated that the solubility of CO_2 in SMMA at 120 °C and 150 °C is more or less similar, and since the driving force for cell growth will be the same at those temperatures, it can also be expected that the foam morphology in terms of density and average cell size will be comparable.

Additionally, the experiments presented in Fig. 5 have been analyzed using Scanning Electron Microscopy (SEM) and subsequently with the developed Voronoi analysis to determine the homogeneity of the obtained morphologies. The results of the analysis can be found in Table 2. Fig. 6A–C displays a selection of SEM pictures of the foams produced at different temperatures and 200 bar. This figure clearly shows an increase in cell size and a decrease in the thickness of the cell walls for increasing temperature, which is consistent with a decrease in density.

Figs. 7A–C and 8A–C show the Voronoi diagrams and cell area distributions corresponding to the SEM pictures of Fig. 6, respectively. Together with the results displayed in Table 2 there appears to be a general trend that the homogeneity decreases with increasing temperature. This trend can be explained by taking a closer look at Fig. 6A, which has been foamed at 93 °C. The cell walls of the foams produced at low temperatures are much thicker as compared to the foams produced at higher temperatures. After nucleation, cell growth will occur. Since these individual cells are relatively far apart, the effect of one cell on the other is negligible. Before the cells have reached a size where they can influence each other, the polymer matrix vitrifies and cell growth stops, resulting in relatively homogeneous foam. At higher temperatures, the cells will interfere with each other by obstruction and will compete for growth. As a result, the cell size distribution will be broader and homogeneity will be less.

3.2.2. Effect of pressure

In order to investigate the effect of the pressure on the density, average cell area, cell area distribution and homogeneity,

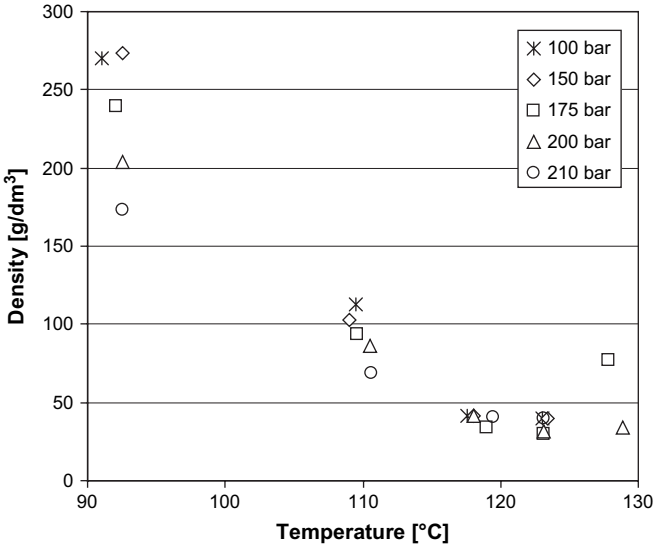

Fig. 5. Density versus the temperature of the SMMA foams produced at various pressures.

Table 2
Results of the SMMA foams produced at different temperatures and pressures and a depressurization time < 1 s

Pressure [bar]	Temperature [°C]	Density [g/dm^3]	Average area Voronoi [μm^2]	HP_A [−]	Number of cells [−]
100	93	271	6015	0.269	118
	110	113	8276	0.323	136
	118	41.3	11,300	0.353	93
	123	39.9	12,037	0.403	82
150	93	273	1016	0.280	858
	110	103	2847	0.313	268
	118	41.8	7474	0.369	156
	123	39.8	12,212	0.378	70
175	93	240	1142	0.251	769
	110	93.8	2131	0.361	379
	118	33.9	4944	0.355	131
	123	29.7	4192	0.346	171
	129	77.0	6938	0.406	85
200	93	204	1121	0.271	777
	110	86.2	3010	0.370	221
	118	31.9	6206	0.452	108
	123	31.7	2918	0.318	276
	129	33.8	6996	0.340	101
210	93	173	–	–	–
	110	68.4	2780	0.423	232
	118	40.7	4117	0.323	182
	123	39.4	3439	0.290	212

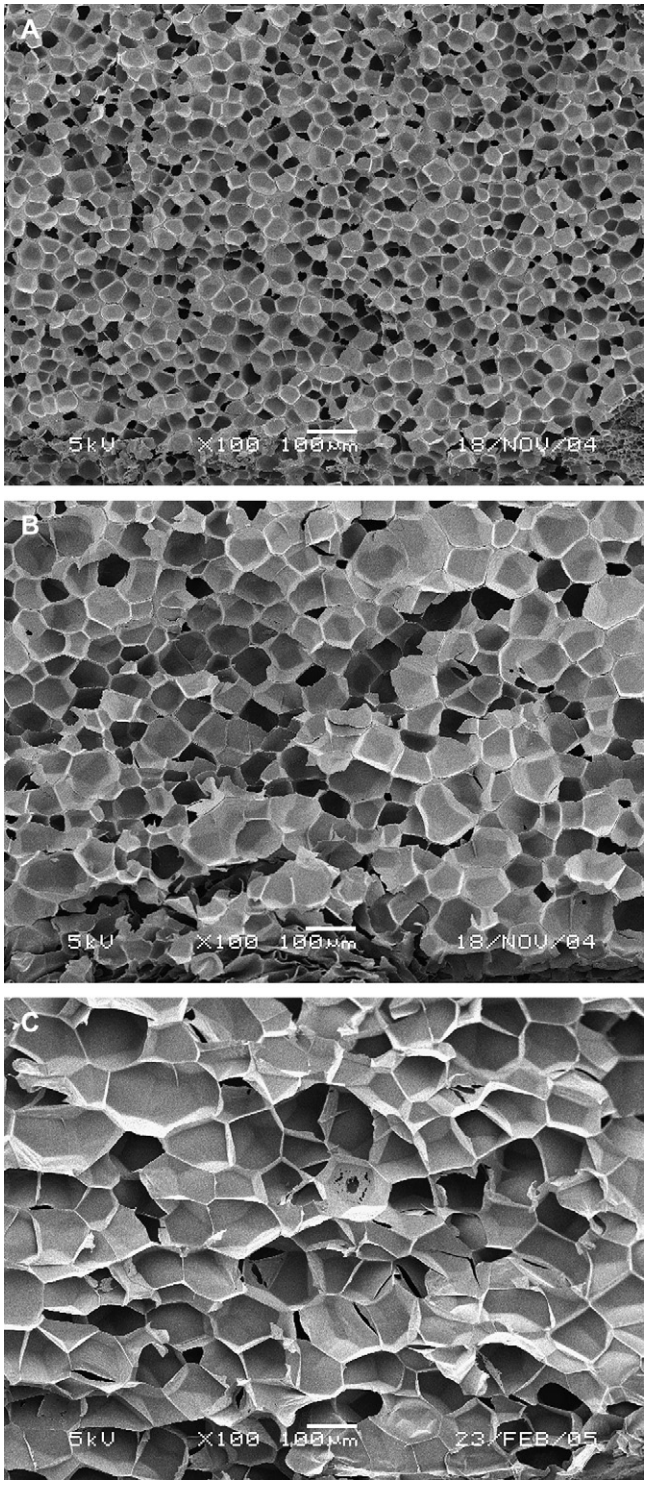

Fig. 6. SEM pictures (100×) of SMMA foamed at 200 bar and (A) 93 °C, (B) 110 °C and (C) 118 °C.

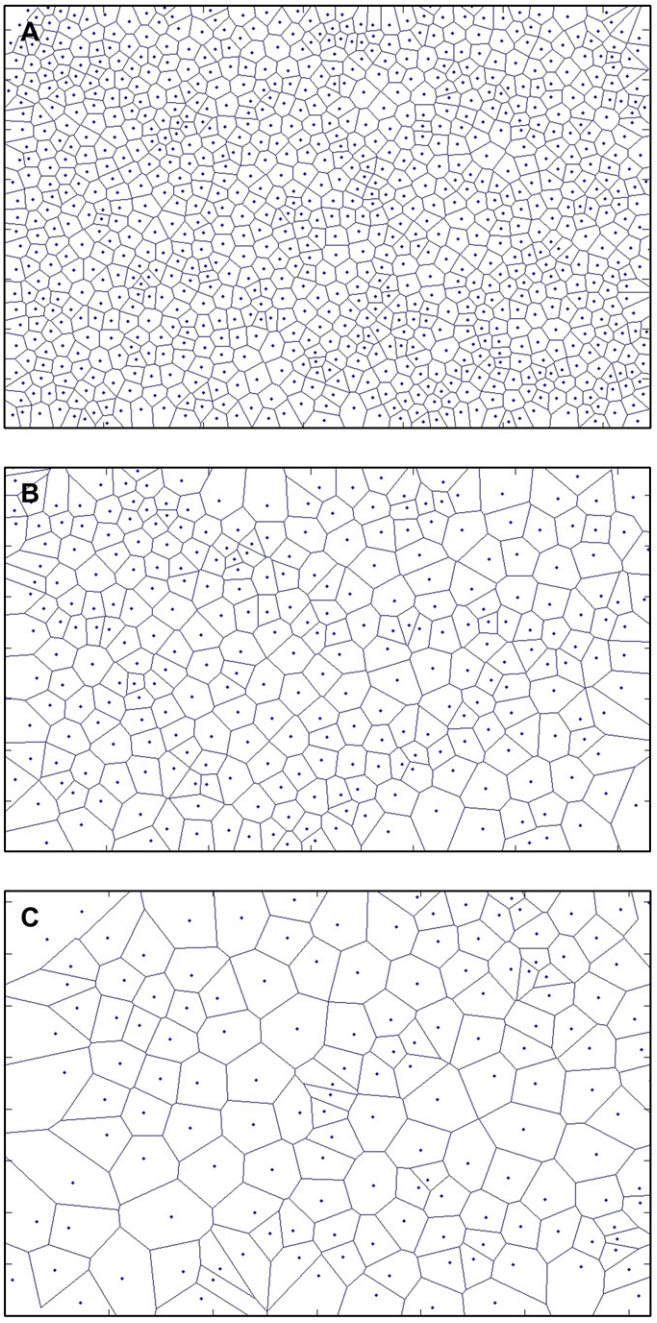

Fig. 7. Corresponding Voronoi diagrams of the SEM pictures presented in Fig. 6.

several experiments have been performed at constant temperature but at different pressures. The effect on the density with increasing pressure is depicted in Fig. 5, which shows that the density decreases upon an increase in pressure. Furthermore, above 118 °C an increase in pressure has no further effect on the density. It can be seen that an increase in pressure appears to have less effect on the density as compared to an increase in temperature. The density decreases only by a factor of 1.2 when the pressure is increased 1.4 times, from 150 bar to 210 bar. However, if the temperature is increased from 93 °C to approximately 130 °C, the density decreases by a factor of 6.8.

Figs. 9, 10 and 11A–C display a selection of the SEM pictures, Voronoi diagrams and cell area distributions of the foams produced at 110 °C and different pressures, respectively. The data are also given in Table 2. It can be concluded that the pressure appears to have little effect on the

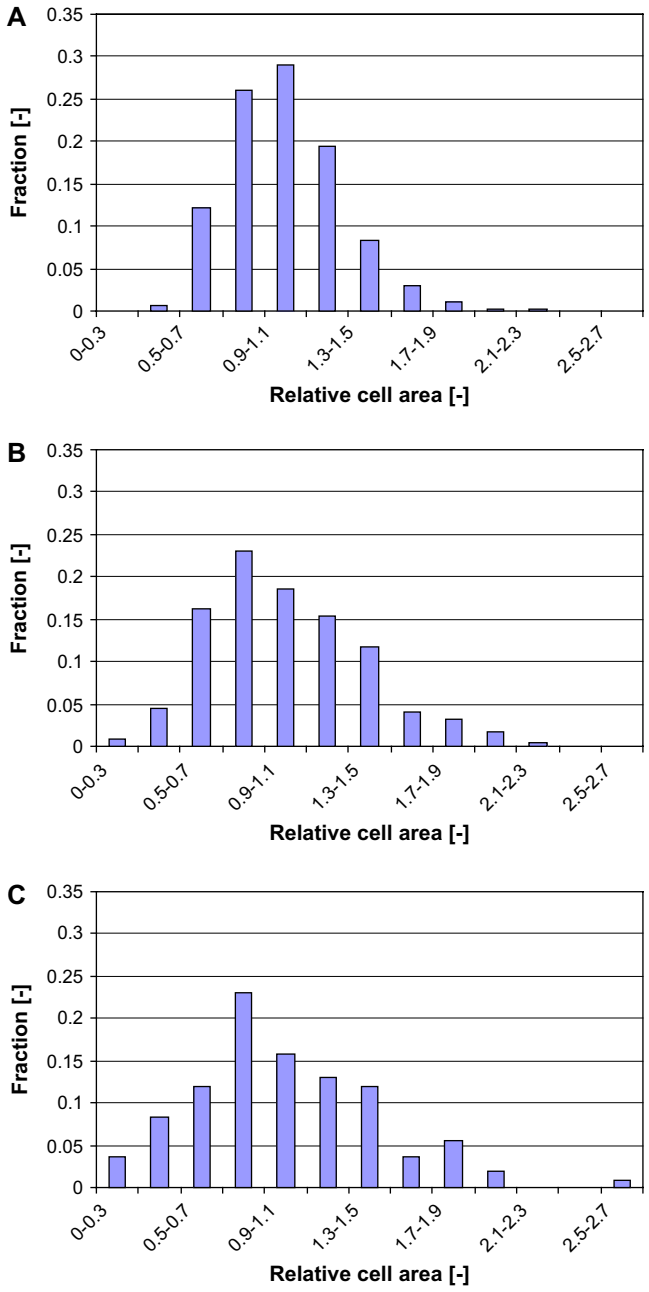

Fig. 8. Corresponding cell area distribution of the Voronoi diagrams presented in Fig. 7.

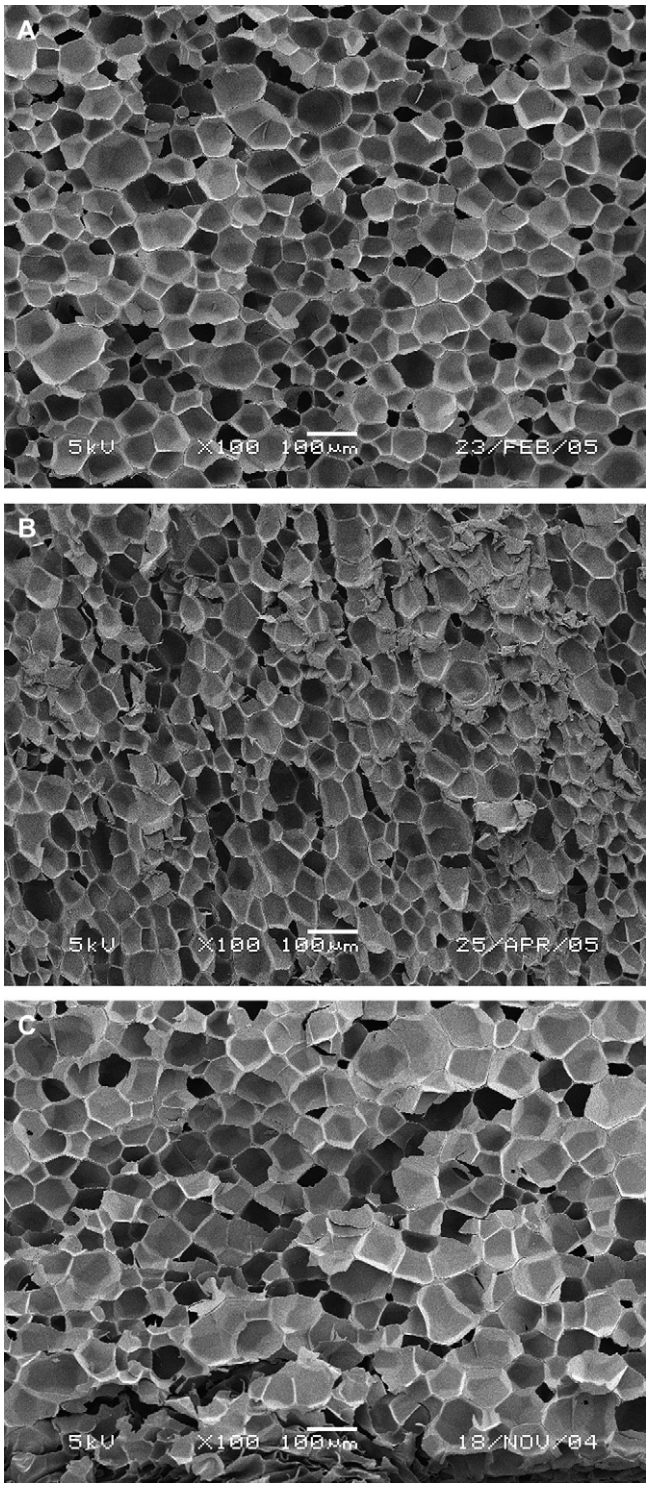

Fig. 9. SEM pictures (100×) of SMMA foamed at 110 °C and (A) 150 bar, (B) 175 bar and (C) 200 bar.

average cell area, which all have the same order of magnitude. However, the cell area distribution broadens with increasing pressure, which results in a decrease of the homogeneity with increasing pressure. This can be explained by the following. As the pressure increases, the amount of CO_2 that can be dissolved in the polymer increases and the glass transition temperature will decrease. Therefore, the effect of the pressure on the foam morphology can considered to be similar to the effect of the temperature. This is confirmed by the results described in the previous paragraph, where an increase in temperature also results in a decrease in density and homogeneity. Due to the fact that the difference in solubility is relatively small, the effect will be less pronounced.

3.2.3. Effect of depressurization rate

To determine the effect of the depressurization rate on the foam morphology, several experiments have been performed

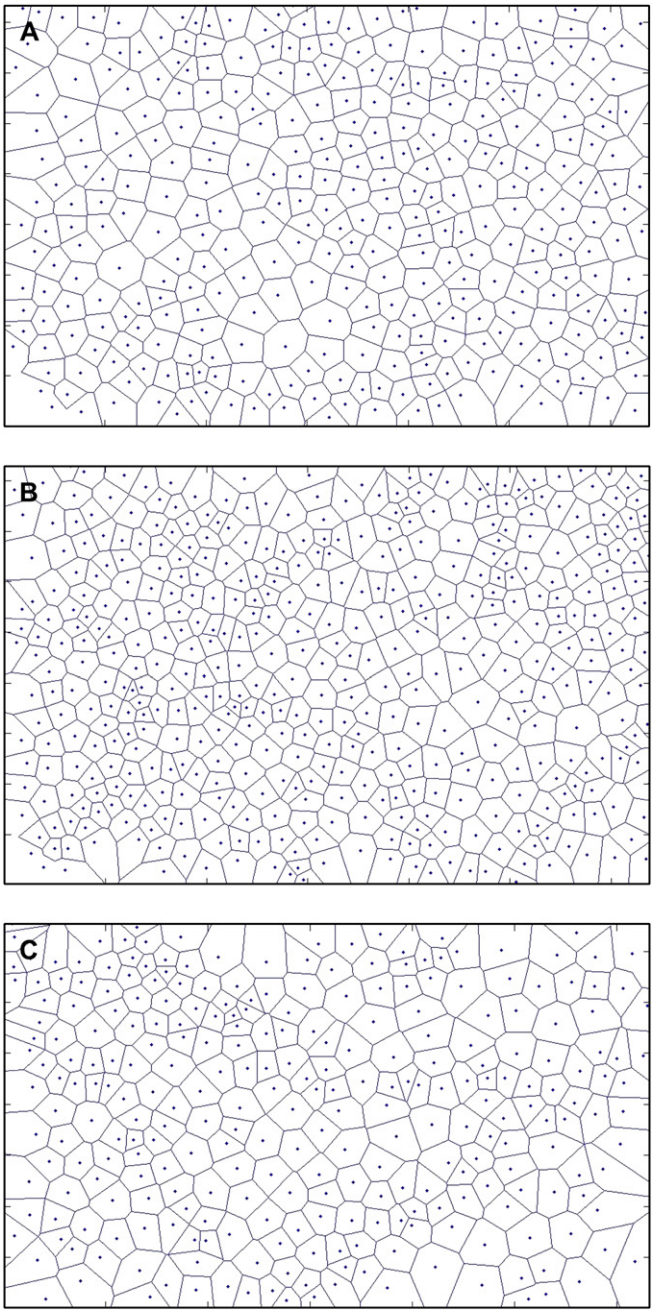

Fig. 10. Corresponding Voronoi diagrams of the SEM pictures presented in Fig. 9.

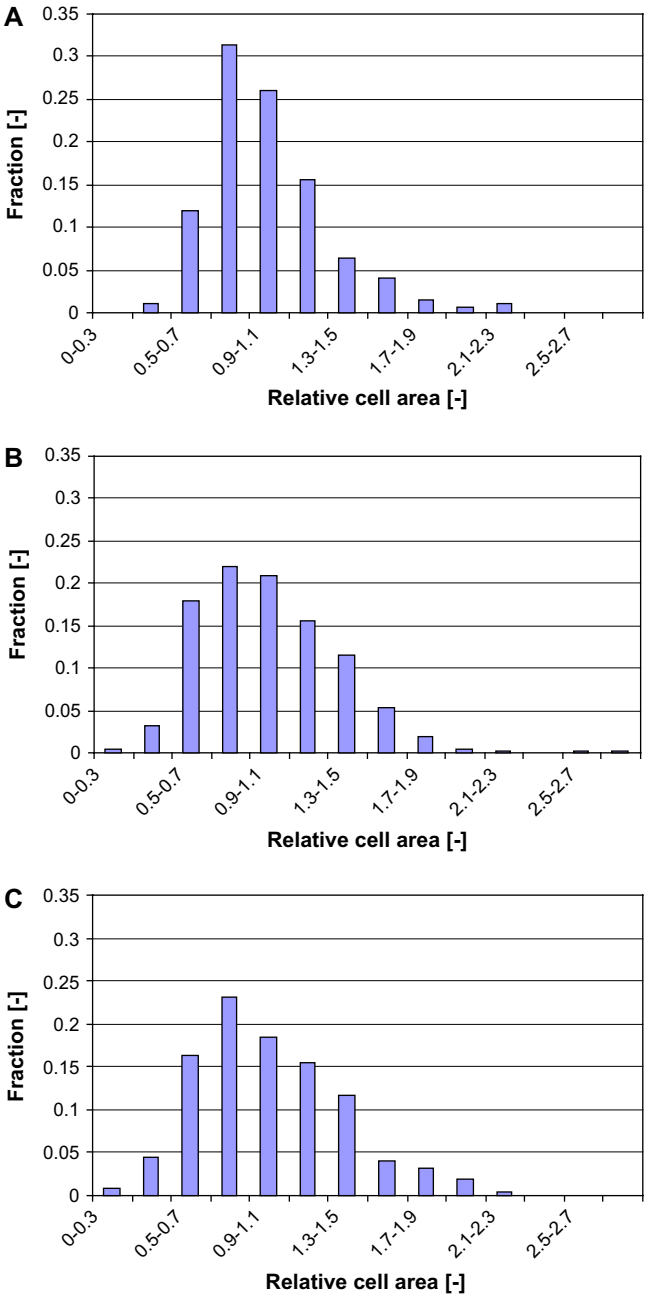

Fig. 11. Corresponding cell area distribution of the Voronoi diagrams presented in Fig. 10.

at a constant saturation temperature of 118 °C and pressure of 200 bar. The time to depressurize the content of the high pressure vessel has been varied from 30 s up to 600 s. The SEM pictures of these experiments with depressurization times up to 230 s are shown in Fig. 12A–D. The pictures show a dramatic increase of the cell size up to approximately 400 μm, already at a depressurization time of 230 s. The increase in cell size with increasing depressurization time has also previously been reported [12,26,27]. Since the cells of the samples with depressurization times above 230 s are too large, it has not been possible to analyse these foams with SEM, even at the minimum magnification. The Voronoi diagrams and cell size distributions corresponding to the SEM pictures of Fig. 12A and B are shown in Figs. 13A and B, 14A and B, respectively. The calculated average area and the homogeneity number are shown in Table 3. Due to the limited number of analyzed cells, the results have less statistical meaning. However, these HP_A numbers are in line with what can be expected, by comparing them to the HP_A numbers of the rapid expansion experiments at the same saturation conditions.

It is expected that the densities for the foams presented in Fig. 12 should be low as well, due to the large cell size.

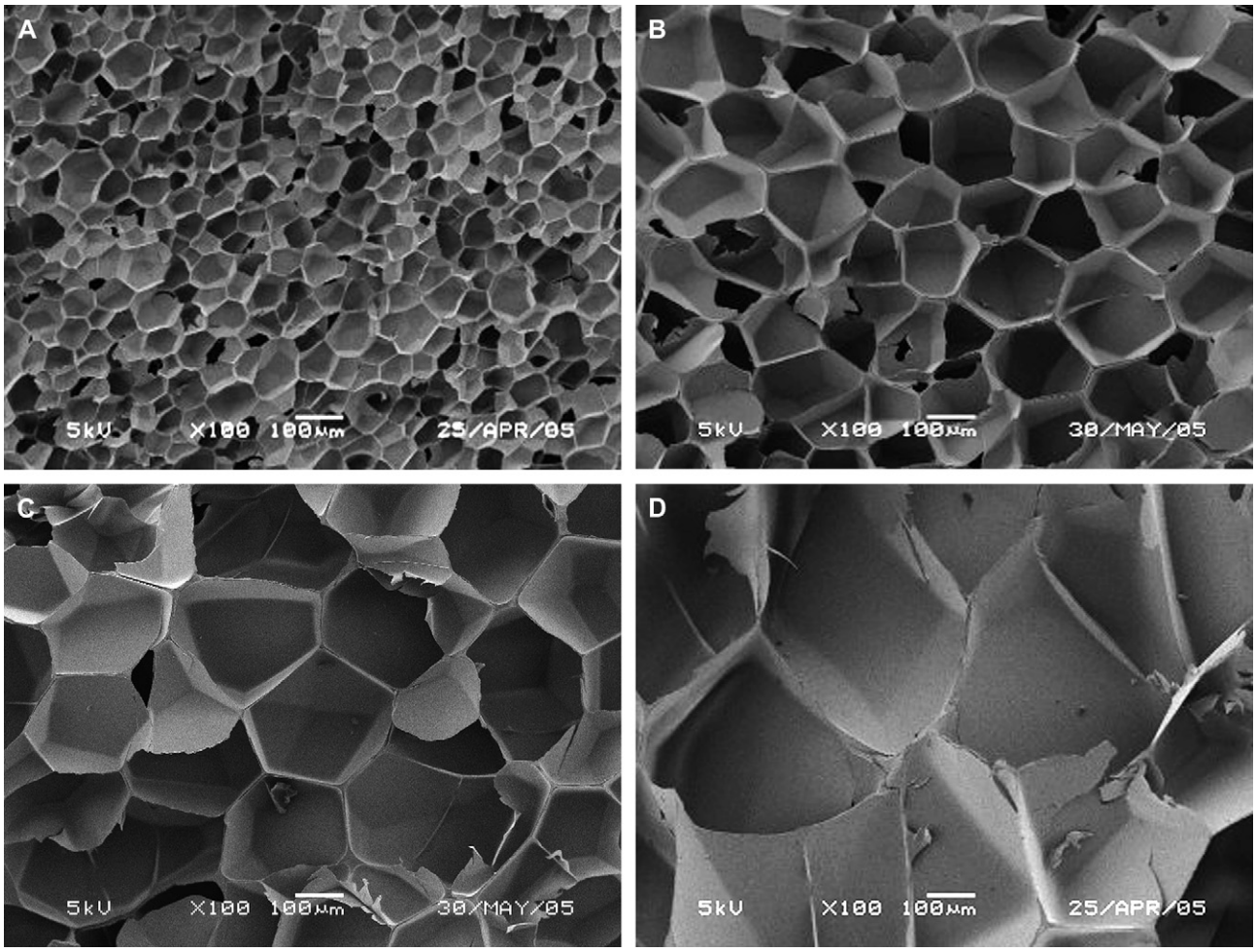

Fig. 12. SEM pictures (100×) of SMMA foams produced at 200 bar and 118 °C, with depressurization times of (A) <1 s, (B) 35 s, (C) 100 s and (D) 230 s.

However, this is not the case. The densities of these foams are higher than the foams of the rapid expansion experiments at the same saturation conditions. Since the total volume of the foamed samples is found to be less and the average cell size is larger, the cell walls of the foams produced at a lower depressurization rate will be thicker. This leads to the observed higher foam densities.

4. Conclusions

It has been shown that a proper selection of the processing conditions allows determining the properties of the resulting foams. Saturation at higher pressures followed by a fast depressurization will lead to a less homogeneous foam morphology, whereas saturation at higher temperatures followed by

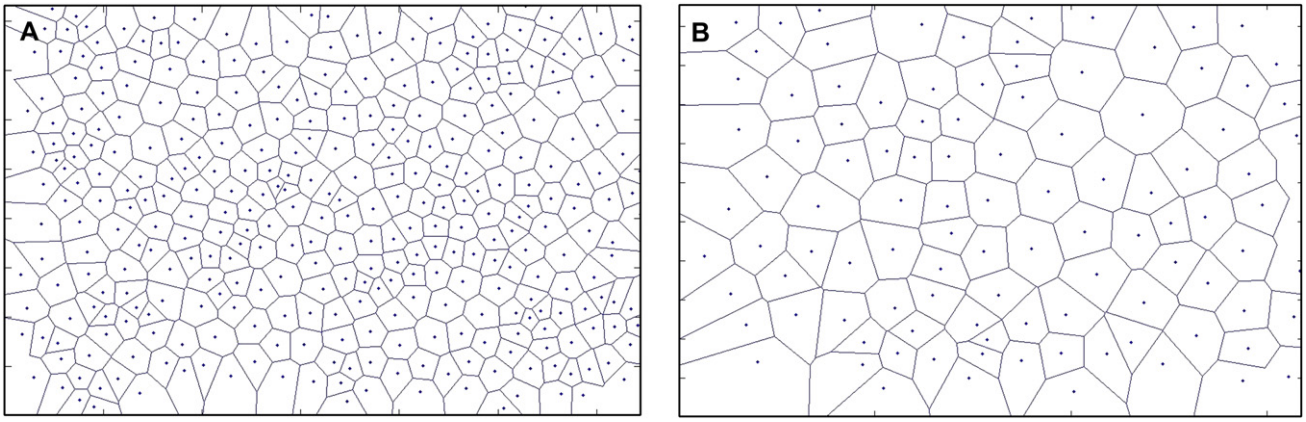

Fig. 13. Voronoi diagrams corresponding to the SEM pictures of Fig. 12A and B.

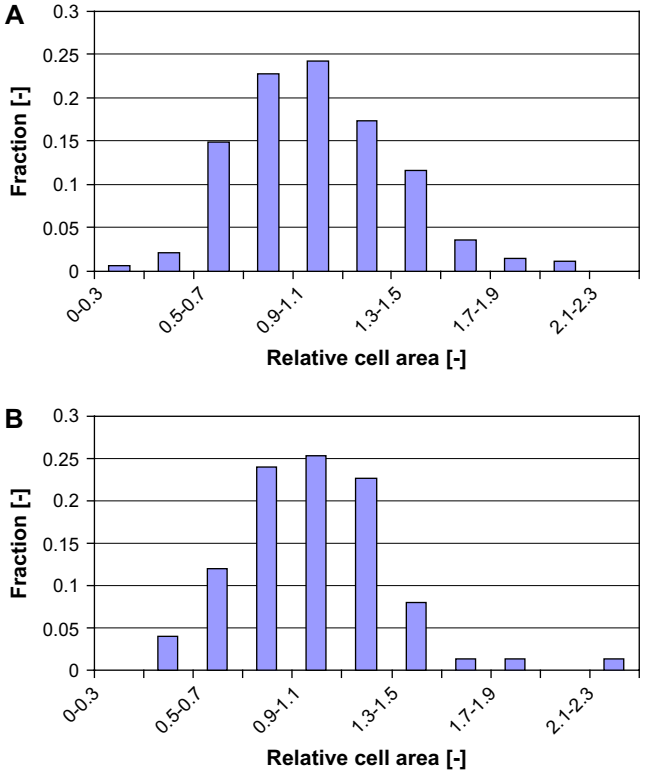

Fig. 14. Cell area distributions corresponding to the SEM pictures of Fig. 12A and B.

Table 3
Characteristic results of the SMMA foams produced at 200 bar, 118 °C and various depressurization times

Time [s]	ρ [kg/m^3]	Average area [μm^2]	HP_A	No. of cells
<1	41.6	2806	0.320	276
35	101	14,034	0.318	75
100	89.0	27,614	0.301	30
230	NA	NA	NA	NA

a fast depressurization will lead to a larger average cell size and a lower density of the produced foam. Also the depressurization rate determines to a large extent the cell size, since the cell size increases with increasing depressurization rate. However, long depressurization times will lead to somewhat higher densities. It has also been shown that saturation at higher temperatures will lead to a broader cell size distribution and less homogeneity. This is due to the fact that at these conditions the cells reach a size where interference by obstruction will occur. As a result the cells will compete for growth.

Based on these conclusions, it can be stated that once the polymer properties, such as the T_g and the solubility of CO_2 are known, full control of the desired foam morphology can be obtained by choosing the correct combination of temperature, pressure and depressurization rate.

Acknowledgements

The authors would like to thank Dr. Ir. Th. W. de Loos of the Delft department of Chemical Technology (DelftChemTech, Delft University of Technology, the Netherlands) and Ir. J. Rooze of the Process Development Group for their useful discussions regarding the Sanchez–Lacombe EOS. The authors would also like to thank Dr. Ing. H.W. Lösch of Rubotherm Präzisionsmesstechnik GmbH (Bochum, Germany) for performing the sorption measurements.

References

[1] Randall D, Lee S, editors. The polyurethanes book. New York: Wiley; 2003.
[2 Tomasko DL, Li H, Liu D, Han X, Wingert MJ, Lee LJ, et al. Ind Eng Chem Res 2003;42(25):6431–56.
[3] Cooper AI. J Mater Chem 2000;10(2):207–34.
[4] Kazarian SG. Polym Sci Ser C 2000;42(1):78–101.
[5] Condo PD, Sanchez IC, Panayiotou CG, Johnston KP. Macromolecules 1992;25(23):6119–27.
[6] O'Neill ML, Handa YP. ASTM special technical publication, STP 1249; 1994. p. 165–73.
[7] Goel SK, Beckman EJ. Polym Eng Sci 1994;34(14):1137–47.
[8] Handa YP, Zhang Z, Nawaby V, Tan J. Cell Polym 2001;20(4):241–53.
[9] Stafford CM, Russell TP, McCarthy TJ. Macromolecules 1999;32(24): 7610–6.
[10] Singh L, Kumar V, Ratner BD. Biomaterials 2004;25(13):2611–7.
[11] Rachtanapun P, Selke SEM, Matuana LM. J Appl Polym Sci 2003; 88(12):2842–50.
[12] Arora KA, Lesser AJ, McCarthy TJ. Macromolecules 1998;31(14): 4614–20.
[13] Loesch HW, Kleinrahm R, Wagner W. Chem Ing Tech 1994;66(8): 1055–8.
[14] Nalawade SP, Picchioni F, Janssen LPBM, Patil VE, Keurentjes JTF, Staudt R. Polym Eng Sci 2006;46(5):643–9.
[15] Sato Y, Yurugi M, Fujiwara K, Takishima S, Masuoka H. Fluid Phase Equilib 1996;125:129–38.
[16] Sato Y, Takikawa T, Takishima S, Masuoka H. J Supercrit Fluid 2001; 19(2):187–98.
[17] Sanchez IC, Lacombe RH. J Phys Chem 1976;80(21):2352–62.
[18] Sanchez IC, Lacombe RH. J Polym Sci Polym Lett Ed 1977;15(2):71–5.
[19] Sanchez IC, Lacombe RH. Macromolecules 1978;11(6):1145–56.
[20] Liu D, Li H, Noon MS, Tomasko DL. Macromolecules 2005;38(10): 4416–24.
[21] Li G, Gunkel F, Wang J, Park CB, Altstädt V. J Appl Polym Sci 2007; 103(5):2945–53.
[22] Jacobs LJM, Danen KCH, Kemmere MF, Keurentjes JTF. Comput Mater Sci 2007;38(4):751–8.
[23] Rodgers PA. J Appl Polym Sci 1993;50(12):2075–83.
[24] Zhang Y, Gangwani KK, Lemert RM. J Supercrit Fluid 1997;11(1–2): 115–34.
[25] Pantoula M, Panayiotou C. J Supercrit Fluid 2006;37(2):254–62.
[26] Jacobs MA, Kemmere MF, Keurentjes JTF. Polymer 2004;45(22): 7539–47.
[27] Liang MT, Wang CM. Ind Eng Chem Res 2000;39(12):4622–6.